Spectroscopic Investigations of Tungsten in the EUV Region and the Determination of its Concentration in Tokamaks

K. Asmussen, K.B. Fournier, J.M. Laming, R. Neu,
J.F. Seely, R. Dux, W. Engelhardt, J.C. Fuchs,
and the ASDEX Upgrade Team

IPP 10/9 November 1997

MAX-PLANCK-INSTITUT FÜR PLASMAPHYSIK

85748 GARCHING BEI MÜNCHEN

MAX-PLANCK-INSTITUT FÜR PLASMAPHYSIK

GARCHING BEI MÜNCHEN

Spectroscopic Investigations of Tungsten in the EUV Region and the Determination of its Concentration in Tokamaks

K. Asmussen, K.B. Fournier, J.M. Laming, R. Neu,
J.F. Seely, R. Dux, W. Engelhardt, J.C. Fuchs,
and the ASDEX Upgrade Team

IPP 10/9 November 1997

Die nachstehende Arbeit wurde im Rahmen des Vertrages zwischen dem Max-Planck-Institut für Plasmaphysik und der Europäischen Atomgemeinschaft über die Zusammenarbeit auf dem Gebiete der Plasmaphysik durchgeführt.

Spectroscopic Investigations of Tungsten in the EUV Region and the Determination of its Concentration in Tokamaks

K. Asmussen, K. B. Fournier[¶], J. M. Laming[*], R. Neu, J.F. Seely[‡],
R. Dux, W. Engelhardt, J. C. Fuchs, and the ASDEX Upgrade Team

Max-Planck-Institut für Plasmaphysik, IPP-EURATOM Association, 85748 Garching, Germany
Email of the ASDEX Upgrade Team: ASDEX.Upgrade@ipp.mpg.de

Abstract

By means of laser ablation tungsten was injected in both ohmic and additionally heated plasmas of the ASDEX Upgrade tokamak experiment. Spectroscopic investigations were performed in the extreme UV (EUV) wavelength region 4–140 nm. Beside the quasicontinuum structure at $\approx$ 5 nm, isolated lines of tungsten were observed in the regions 4.5–6 nm and 12–14 nm. By comparison with calculations from the HULLAC and RELAC codes, these lines could be identified as transitions of Br– to Ni–like tungsten ions. The concentration c_W of tungsten after laser ablation was determined from comparisons between the total tungsten radiation P_W and calculated radiation losses. Calibration of the quasicontinuum intensity with the help of the P_W measurements allows to determine the tungsten concentration from spectroscopic observations, which are more sensitive. Both concentration measurements (quasicontinuum, P_W) agree well in discharges with laser ablation . From a comparison of the intensity of the isolated lines with code results, c_W could be estimated in the central region of hot, additionally heated plasmas. The lower detection limit of the spectroscopic method allows the extraction of c_W during the tungsten divertor experiment of ASDEX Upgrade.

¶ Lawrence Livermore National Laboratory, Livermore, California 94550, USA
* SFA Inc, Largo MD 20774, and E. O. Hulburt Center for Space Research, Naval Research Laboratory, Code 7674L, Washington DC 20375
‡ E. O. Hulburt Center for Space Research, Naval Research Laboratory, Code 7674S, Washington DC 20375

1 Introduction

High particle and energy fluxes in future fusion experiments demand the investigation of materials for plasma facing components [1]. A promising alternative to the now-a-days frequently used low-Z-materials carbon and beryllium is tungsten. Due to its high mass, tungsten's sputtering rate is comparatively low, and unlike carbon, there is no chemical erosion [2]. The disadvantage of tungsten is the high specific radiation losses [3] if the element penetrates into the central plasma region. During the tungsten limiter experiment at PLT [4] the high W radiation led to hollow temperature profiles. In divertor experiments, however, the temperature in front of plasma facing components can be made much lower and therefore the tungsten source caused by erosion should also be much smaller. At ASDEX Upgrade the divertor plates were therefore coated with tungsten to test the suitability of this element for future fusion experiments [5].

The dependence of the tungsten concentration c_W in the main plasma on other plasma parameters is in this context of major interest. To investigate the behaviour of W in the plasma the element has to be identified and methods for the determination of its concentration have to be developed. With the help of laser ablation studies the spectral emissivity of W in the wavelength region 5 nm to 140 nm was investigated. The region at about 5 nm proved to be especially suitable for investigation, since radiation from tungsten ions can be observed over a large temperature range in this region. The concentration of W was first derived in discharges with laser ablation from a comparison of the total tungsten radiation with calculated radiation losses. To improve the detection limit of c_W, the spectroscopic measurements of the quasicontinuum structure (which is emitted in the $T_e \approx 1$ keV shell of a discharge) were developed as diagnostics by calibrating the signal against the concentrations derived from the measured total tungsten radiation in plasmas with laser ablation. The increased signal-to-noise-ratio of the spectroscopic method allows a detection of W down to $c_W \leq 10^{-5}$. To extend the concentration measurements to plasma regions with temperature $T_e \geq 1.5$ keV, the grazing incidence spectrometer used in the present experiments was absolutely calibrated at 6 nm by means of a double branching ratio. From the calibrated intensity of the line of Cu-like tungsten at λ=6.23 nm and data from the HULLAC-Code [6,7] c_W can also be determined in additionally heated plasmas.

2 Experimental Setup

The tungsten was injected by means of laser ablation (about 10^{17} atoms/laser pulse) in ASDEX Upgrade [8]. Due to the high temperature in the main plasma the tungsten ions reach ionization stages of W^{20+} and higher and the radiation of the element occurs mainly in the VUV-, EUV- and x-ray-region.

The radiation in the EUV-region from 4 nm to 30 nm was observed with the help of a 2.2 m grazing incidence spectrometer [9]. The line of sight of the spectrometer looks almost horizontally through the plasma center of ASDEX Upgrade. The plasma radiation is diffracted and focused by a 600 grooves/mm-grating and observed by means of a multi channel plate system, consisting of a single MCP, a phosphor screen, a fiber guide, and a photo diode array. At about 5 nm a wavelength range of 3 nm can be viewed simultaneously with a time resolution of Δt=5 ms and a wavelength resolution of about $\lambda/\Delta\lambda \approx 150$. By shifting the MCP along the Rowland circle the spectral range can be tuned from 4 nm up to 60 nm.

The calibration of the grazing incidence spectrometer was done by means of a double branching ratio method. The transitions used are

1. $2s^2 3s\ ^2S_{1/2} - 2s^2(^1S)3p\ ^2P_{1/2}$ (CII, $\lambda \approx 658$ nm) $\Leftrightarrow$ $2s2p^2\ ^2S_{1/2} - 2s^2(^1S)3p\ ^2P_{1/2}$ (CII, $\lambda \approx 237$ nm)
2. $1s2s\ ^3S_1 - 1s2p\ ^3P_1$ (BIV, $\lambda \approx 282.6$ nm) $\Leftrightarrow$ $1s^2\ ^1S_0 - 1s2p\ ^3P_1$ (BIV, $\lambda \approx 6.1088$ nm)

With the assumptions that the emission is homogeneous from the point of view of the spectrometers used and toroidally symmetric, first a UV/visible spectrometer with the same line of sight as the grazing incidence spectrometer (but other toroidal location) was calibrated at $\lambda \approx$237 nm. In a second step the grazing incidence spectrometer was calibrated by means of the second line pair and comparison with the UV spectrometer.

For the observation of the VUV wavelength region a SPRED spectrometer (survey, poor resolution, extended domain) was used [10]. This spectrometer offers the possibility to observe simultaneously the whole spectral range from 10 nm to 140 nm with the reduced resolution of $\Delta\lambda \approx$0.5 nm. The line of sight of both spectrometers are shown in fig. 1, left side. The X-ray measurements are described elsewhere [11].

The spatial distribution of the total tungsten radiation was investigated with a bolometer camera system (cf. fig. 1, right side). It consists of a vertical and a horizontal camera system with 24 and 40 single channels, respectively. The cameras integrate the intensity of the radiation emitted in the wavelength region from 0.1 nm to 200 nm. The time resolution of the system is Δt=1 ms. A deconvolution algorithm is used to get the radiation density distribution in the poloidal plane of the plasma [12].

Temperature profiles were obtained every 10 ms to 20 ms by means of a Thomson scattering system, the electron density profiles were derived with the help of a DCN interferometer system (Δt=0.1 ms).

3 Spectroscopic Investigations

For spectroscopic investigations, W was injected by means of laser ablation, which allows study of emission from different tungsten ions by observing the time evolution of the spectra. From the ionization energies of the W ions [13] the maximum charge expected on the tungsten ions can be estimated to be about 30 in ohmic discharges (heated only by the plasma current, central electron temperature $T_{e,0} \approx$ 1 keV) and about 50 in discharges with neutral beam heating ($T_{e,0}$ = 2-4 keV).

Identification of the line features observed in the present work is achieved by comparison with *ab initio* calculations of level energies and predictions of the collisional-radiative line emissivities. The atomic structure calculations for the level energies are done with the graphical angular momentum coupling code ANGLAR [14] and the fully relativistic parametric potential [15] code RELAC of Klapisch *et al.* [6]. ANGLAR uses the graphical angular recoupling routine NJGRAF [14] to generate fine structure levels in a jj-coupling scheme for a set of user-specified electron configurations. RELAC then calculates the multiconfiguration, intermediate coupling level energies for each ion. RELAC also computes the transition rates and oscillator strengths for any multipole operator [16] requested.

The HULLAC package (Hebrew University Lawrence Livermore Atomic Codes) includes ANGLAR and RELAC, as well as the CROSS [7] suite of codes; HULLAC produces the data necessary to compute the population in the levels of a given ion. CROSS uses RELAC's wavefunctions to compute distorted wave approximation collisional excitation rates between all the levels of a given ion. CROSS is able to accomplish this using the factorization theorem of Bar-Shalom, Klapisch and Oreg in conjunction with a semi-empirical interpolation scheme [7]. The collision rates and the electric and magnetic dipole and quadrupole transition (E1, M1, E2 and M2, respectively) probabilities are then used to find the steady state collisional-radiative level populations (and thus, line intensities) in each ion. Further details about the calculation of the collisional-radiative spectrum for each tungsten ion in the present work can be found in Ref. [17].

3.1 Tungsten quasicontinuum

In ohmic discharges only the known quasicontinuum structure of tungsten at about 5 nm was observed in the EUV and VUV region (4 nm to 140 nm) [4, 18, 19]. It is caused by tungsten ions with open 4d and 4f subshells (W^{27+}, etc.). The great number of coupling possibilities of the bound electrons leads to a large number of energy levels with similar energies, resulting in an array of lines. Furthermore the arrays of different tungsten ions overlap in the same wavelength region. The emission from these ions has been studied by Finkenthal *et al.* [18] and Mandelbaum *et al.* [19] using the Unresolved Transition Array formalism.

The main contribution to the quasicontinuum is emitted from W ions around the Ag-like W^{27+} ion [20–22]. This is confirmed by the dependence of the quasicontinuum intensity on temperature and the occurrence of individual lines of Ag-, Pd-, and Rh-like ions in discharges with tungsten accumulation after W laser ablation. Figure 2 shows a plot of the maximum of the intensity of the W quasicontinuum after tungsten laser ablation normalized to the line averaged electron density and maximum central tungsten concentration $c_{W,bolo}$ as a function of the central temperature. The normalization on $c_{W,bolo}$, determined by means of the bolometer system and theoretical radiation loss calculations (cf. section 4.1), was carried out to correct the intensity for the influence of different numbers of injected tungsten atoms and different plasma transport properties. The increase of the intensity at low temperatures is caused by the fact that a certain minimum temperature is needed to produce the quasicontinuum emitting tungsten ions. The decrease at higher temperatures is caused by the decreasing thickness of the plasma shell in which these ions exists due to its shift outwards, towards the plasma boundary.

A simple model can give a rough explanation of this temperature dependence. It is assumed that:
1. the quasicontinuum radiation is mainly emitted by a few ionization stages existing within the temperature range $T \approx T_m \pm \Delta T$,
2. the resulting emission ε can be approximated by a gaussian dependence on temperature ($\varepsilon \sim \exp(-(T-T_m)^2/(2\cdot\sigma^2))$ with $\sigma = \sqrt{2 \cdot \ln 2} \cdot \Delta T$) and
3. the temperature profile is similar for different discharges. With a peak emission at $T_m \approx 950$ eV and a FWHM of $2 \cdot \Delta T \approx 550$ eV the solid curve in fig. 2 is obtained.
A calculation using the STRAHL transport code (fig. 9, cf. 3.3) shows that the corresponding ions have charges similar to the Ag–, Pd–, and Rh–like tungsten ions ($E_{ion,Pd\text{-}like} \approx 1150$ eV [13]), which agrees with the results of [21].

In a few discharges an accumulation of tungsten in the central plasma after laser ablation occured, which offered a second test for the identification of the source of the quasicontinuum radiation. Accumulation is usually defined as strong peaking of the impurity concentration, compared with the electron density profile. It is caused by a high central particle confinement and an inward drift of the impurity ions. The definition of accumulation in connection with laser blow off is more difficult. This is due to the fact that even in the case of a simple diffusion process with a constant radial diffusion coefficient the profile of the impurity density becomes automatically peaked when the source at the plasma boundary is switched off. Therefore in this case more emphasis has to be put on the particle confinement time, i.e. accumulation of tungsten after laser ablation means that the tungsten concentration becomes very high and the element stays in the plasma for a long time.

The resulting high tungsten radiation losses in these accumulation discharges lead to flat or almost hollow temperature profiles. An example of the temporal evolution of W spectra during accumulation is shown in fig. 3. The discharge corresponds to the accumulation point at 800 eV in fig. 2 (NBI: 2.5 MW,

I_p = 1 MA , $\bar{n}_e = 6.5 \cdot 10^{19}$ m^{-3}). After injecting W into the plasma at 3 s the usual quasicontinuum structure is observed (Δt= 35 and 100 ms). The large additional radiation losses due to tungsten of about 1 MW in the main plasma cause a temperature drop from $T_{e,0} \approx$ 2.5 keV to about 900 eV, resulting in a hollow temperature profile. The distributions of the Ag–, Pd–, and Rh–like ions (W^{27+},W^{28+},and W^{29+}, respectively) get broader, the intensity of the lines emitted by these ions increases ($\Delta t \geq 150$ ms) and isolated lines can be distinguished from the rest of the quasicontinuum. The tungsten remains in the plasma longer than 500 ms ($\tau_{decay} > 1000$ ms). When the NBI is switched off, a minor disruption occurs, the particle confinement decreases (H- to L-mode transition) and the tungsten diffuses out of the plasma.

Table 1 in the appendix shows the identification of some lines according to [21]. Other lines in the spectrum could not be identified, because the resolution of the grazing incidence spectrometer is insufficient.

3.2 Isolated lines of higher ionized tungsten

In hot plasmas with temperatures about 2 keV isolated tungsten lines can be observed in the wavelength region from 4 nm to 15 nm. In the region above 15 nm no lines were found. The region from 4 nm to 7 nm was monitored more often, because it offers the possibility to detect simultaneously the quasicontinuum structure and the line features.

Figure 4 shows the temporal development of the spectrum of the grazing incidence spectrometer in a discharge with 7 MW NBI additional heating power (#4896, $\bar{n}_e \approx 8 \cdot 10^{19}$ m^{-3}, $T_{e,0} \approx$2.4 keV, I_p=1 MA). Immediately after tungsten ablation the quasicontinuum rises and reaches a maximum after about 20 ms. As the tungsten ions penetrate deeper into the plasma they reach regions with higher temperatures. Ions with larger charge numbers occur and radiate strong isolated lines (marked in fig 4).

Characteristic of these additional lines is the temporal development of their intensities. The sawtooth-shaped behavior indicates that they are emitted from the hot core plasma by highly ionized tungsten ions. The variation in intensity is a result of the internal sawtooth–instability, which periodically ejects particles and energy out of the central plasma. Because of the lowered T_e the tungsten ions recombine and become less ionized. Along with recombination in the cooler plasma, the tungsten is distributed over a larger plasma volume that cannot be completely observed by the grazing incidence spectrometer. Both effects lead to a reduction of the observed intensity of the isolated tungsten lines. After the sawtooth–crash the element accumulates again in the central plasma and the cycle starts over again.

A spectrum of the lines 200 ms after the W-injection of the same discharge is shown in fig. 5, B. The total exposure time was 100 ms, the background radiation is subtracted. The upper spectrum (A), which serves for the wavelength calibration, was detected at the beginning of the discharge. It shows lines of boron (BIV: $1s^2$ – 1s2p and BV: 1s – 2p) and carbon (2.ord. CVI:1s – 2p) [23]. The error of the peak position of isolated lines is estimated to be 0.01 nm. The identification of the W lines was performed by comparison with observations in [24–26] and with the help of HULLAC-code calculations. The calculated spectrum (in which the spectra of the single W ions were shifted by an amount of up to 0.03 nm to longer wavelengths) is shown in the lower part of the figure (C). The element symbols in spectrum B indicate the isoelectronic sequences to which the corresponding tungsten ions belong to (Br– to Cu–like ions, W^{39+} – W^{45+}). Strong lines are radiated by tungsten ions isoelectronic to Cu, Zn, and Ga, because of their relative simple electron configuration; there are only a few resonant transitions in each ion. The lines are listed in Table 3 (appendix).

Other lines of the same ions were found in the wavelength region from 12 to 14 nm, whereas in the region from 7 to 12 nm no lines were evident. Tungsten was injected both in an ohmic (#7470, $\bar{n}_e \approx 4 \cdot 10^{19}$ m^{-3}, $T_{e,0} \approx 1$ keV, I_p=1 MA) and an additional heated (5 MW NBI, $\bar{n}_e \approx 6 \cdot 10^{19}$ m^{-3}, $T_{e,0} \approx 2.6$ keV) plasma phase. In the ohmic phase (not shown) no tungsten lines were observed, whereas during the neutral beam injection, with higher temperatures, isolated lines occured after laser ablation. Figure 6 shows the temporal behaviour of the grazing incidence spectra (inset A, fig. 6), the time-averaged spectrum (integration period 60 ms – 150 ms after W ablation, (inset B), and the result of the RELAC-Code (insets C). The sawtooth–like temporal behaviour of the line intensities (cf. inset A) and the high $T_{e,0}$ suggests that these lines are emitted by the same ions as the lines in the 5 nm–region. Due to the lack of calibration lines in this spectral range the wavelengths in this region are more uncertain than in the 4–7 nm–region (estimates: $\Delta\lambda_{shift} \leq 0.2$ nm, $\Delta(\lambda_1\text{-}\lambda_2) \leq 0.02$ nm).

Table 4 (appendix) lists the wavelengths and probable transitions of the lines of spectrum B, which results from a comparison with C. The lines 1–4 are 2nd order diffractions of the lines at lower wavelengths. The height of a feature in the synthetic spectra of fig. 6. C is determined by a calculation [17] of the collisional-radiative intensity of the lines in each ion; the intensities are relative to other lines only from the same charge state. The calculation of the collisional-radiative spectrum of each ion is necessary since many of the lines identified in Table 4 are electric dipole (E1) forbidden. The high intensity of a magnetic dipole (M1) or electric quadrupole (E2) line is due to high population in its upper state; the populations are only revealed by the collisional-radiative model. The calculated wavelength of the Zn-like W^{44+} line observed at 13.35 nm is very sensitive to configuration interaction (CI) in the energy level calculation [6]. Other calculations [17,27] that account for CI between the ground level of the Zn-like ion ($4s^2\ ^1S_0$) and doubly excited levels from configurations such as $4p^2$, $4d^2$ and $4p4f$ produce wavelengths shorter than that reported in Table 4; the calculated wavelength (13.399 nm) of the present work neglects the above mentioned CI. To our knowledge, this transition in Zn-like W^{44+} has not been observed before.

3.3 Calculated ion distributions

To derive tungsten concentrations from the observed W radiation in a discharge, the radiation losses of tungsten, the relative abundances of the W ions and the thickness of the corresponding plasma shells were calculated by means of the ADPAK-package [3] and the transport code STRAHL [28]. The required rates for ionization, radiative and dielectronic recombination are included in the ADPAK-package. A comparison of observed tungsten spectra in different types of discharges with theoretical W ion distributions offers the possibility to check these rates.

Whereas the dependence of the intensity of the W quasicontinuum on T_e (fig. 2) is consistent with the calculated distribution of Ag- to Pd-like W ions, the observation of Cu-like tungsten in additionally heated plasmas with $T_e \approx 2.3$ keV cannot be explained by the original ADPAK rates. To get agreement between spectroscopic observations and STRAHL predictions, the ionization rates for W ions with charge numbers larger 30 had to be increased by a factor of up to 3. The same result could have been obtained by decreasing the recombination rates with the same factor. Calculations by Mitnik *et al.* [29,30] can explain the increase of the ionization rates by excitation autoionization. A comparison of the different ionization rate coefficients for Zn- and Cu-like tungsten ions is given in fig. 7. Thick solid lines are the ionization rates ultimately used in STRAHL, thin solid lines represent unmodified ionization rates from ADPAK, and the dashed lines are the sum of ADPAK- and excitation autoionization rates. By inclusion of excitation autoionization the difference between the theoretical total ionization rate and the ionization

rate needed to reproduce the measurements is reduced from a factor of 3 to a factor of 1.4 (= 40%, i.e. good agreement within the uncertainties of the modification factors).

Figure 8 shows the relative abundances of some W ions, calculated with different assumptions for a typical ASDEX Upgrade discharge with NBI-heating (neutral beam injection) ($n_{e,0} = 8{\cdot}10^{19}$ m^{-3} ; $T_{e,0} = 2.6$ keV; pure diffusive transport with a smoothly varying diffusion-profile: $D_{\rho_{pol}=0}= 0.5$ m^2/s, $D_{\rho_{pol}=0.8}= 2.5$ m^2/s, $\rho_{pol} \approx r/a$=normalized small radius, cf. [31]). Thin solid lines represent the results from unmodified ADPAK rates for ionization and recombination. In this case the maximum charge state of tungsten is about 42, which is insufficient to explain the occurrence of lines of Cu- and Zn-like W ions. Thick solid (dashed) lines indicate modified rates of ionization (recombination). The results do not differ very much, but the modified ionization rates are used because of excitation autoionization effects. The ion distribution calculated for a coronal ionization equilibrium without transport can be seen from the thin dashed lines. The influence of the transport on the distribution is very small, and thus, is excluded as a possible explanation for the observation of the lines of 45 times ionized W.

In Fig. 9 the distribution of all W ionization states is shown (determined with the help of the modified ADPAK-rates). In discharges with comparable central temperatures $T_{e,0}$ tungsten ions with simple electron configurations (Kr- to Cu-like tungsten, $4s^2 4p^m$ or $4s^n$) can be found in the plasma center. Tungsten ions with charge numbers similar to Ag-like tungsten (W^{27+}), which emit a quasicontinuum structure at about 5 nm, are located at the outer half of the plasma ($\rho_{pol} \approx 0.7$). In ohmic discharges only ionization states up to $\approx W^{30+}$ can be found in the plasma, because of of the lower electron temperatures. These calculated distributions of the W ionization states are in qualitative agreement with calculations of the ionization equilibrium given in [32]. To get a simpler representation of the modified ADPAK-rates the data arrays were fitted to commonly used formulae for the different rate coefficients. Table 5 in the appendix shows the used formulae, the fit coefficients for the used rates, and the multiplier factors of the ionization rates.

4 Determination of the Tungsten Concentration

4.1 Total Tungsten Radiation

The basis for the determination of the tungsten concentration in the main plasma of ASDEX Upgrade is the additional tungsten radiation after laser ablation. From a deconvolution of the line of sight intensities of the bolometer camera channels the spatial distribution of radiation is obtained. Averaging this radiation over magnetic flux surfaces gives radial radiation profiles. With the assumption that the tungsten injection does not modify the background radiation (the amount of ablated tungsten has to be small enough) a subtraction of the radiation immediately before the tungsten laser ablation from all following profiles yields radial tungsten radiation profiles.

Assuming an ionization equilibrium near to coronal ionization equilibrium for the tungsten ions in the main plasma, the inversion of

$$P_W = n_e(r,t) \cdot n_W(r,t) \cdot p_W(r,t) \qquad (1)$$

yields the tungsten density n_W and concentration $c_W = n_W/n_e$ as a functions of time and the minor plasma radius. In this equation P_W is the radiation loss due to tungsten, $n_e(r)$ the electron density profile, and $p_W(T_e(r,t))$ the calculated radiation loss parameter of tungsten [3] (cf. fig. 10, A). In the following c_W determined by means of this method will be denoted as $c_{W,bolo}$.

The magnitude of the error of n_W is determined by the validity of the coronal ionization equilibrium, the uncertainties of the deconvolution algorithm, the error of the profiles of electron temperature and density, and the error in the calculation of $p_W(T_e)$.

The assumption that the distribution of the tungsten ions obeys the coronal ionization equilibrium is justified in the main plasma of ASDEX Upgrade because the transport time of the W ions is sufficiently large compared to the ionization time (cf. fig. 8). Furthermore, a small deviation of the actual ion distribution from the coronal equilibrium does not change the radiation losses very much, because tungsten ions with similar charge numbers radiate with comparable intensity in the same spectral bands.

Uncertainties in the deconvolution procedure and the subtraction of the background radiation have a direct influence on the total error of c_W. From a comparison of the deconvoluted plasma radiation profiles of several discharges with tungsten laser ablation, this error is estimated to be about 30% for peaked radiation profiles. If hollow profiles occur (in discharges with high tungsten confinement times) the errors in the central part become larger.

A third source of errors are the profiles of electron temperature and density. Whereas the temperature influences the concentration measurements only indirectly through the specific radiation losses $p_W(T_e)$, the electron density profile enters the calculation as multiplicative factor. The uncertainties of the profiles are estimated to be about 20%.

The error in the calculation of $p_W(T_e)$ is more difficult to estimate. In the region with $T_e \approx 1$ keV a comparison with the absolutely calibrated measurements of the grazing incidence spectrometer at $\Delta\lambda = 6$ nm (cf. section 4.3) suggest an relative error $\delta p_W \leq 30\%$. For the temperature region above $T_e = 1.5$ keV (additionally heated plasmas) the necessary changes of the ionization rates (discussed in § 3.3) will probably result in a larger error in p_W (which was calculated with the unmodified rates).

The resulting total relative error of $c_{W,bolo}$ for central measurements in ohmic discharges can be estimated $\delta c_{W,bolo} \approx \delta \bar{n}_e + \delta p_W + \delta P_W \approx 0.2 + 0.3 + 0.3 \approx 0.8$. The detection limit of this method is determined by the need to subtract the background radiation of the plasma and the deconvolution errors. Below $c_W \approx 10^{-4}$ the errors are found to be too large to give reliable results.

To check the determined c_W the maximum inventory of tungsten after laser ablation inside the ρ=0.6 flux surface ($= \int c_W(\rho)\, dV$) was compared with the injected amount of tungsten (see fig. 10, right side). To simplify the automatic determination of n_W parabolic profiles for electron density and temperature were used. The temperature at the boundary (ρ_{pol}=1.0) was assumed to be 10% of $T_{e,0}$, the density at the boundary was estimated to be 90% of the central value $n_{e,0}$. The volume was limited to ρ=0.6 ($\approx$1/3 of the total plasma volume), because at larger radii the errors due to profile deviation and $p_W(T_e)$–variations are too high (the density– and $p_W(T_e)$– gradients are large at the plasma boundary). In the majority of the discharges the maximum inventory is found to be 4% to 14% of the ablated amount of W. With the rough assumption of a constant tungsten density in the main plasma a total plasma inventory of 12%–42% of the injected amount of tungsten can be estimated. This value is consistent with other investigations of laser ablation experiments [33]. The variation of the ratio between the measured tungsten concentration and the injected amount of the element demonstrates large variations in the main plasma transport, which depends very sensitively on several plasma parameters (the same sensitivity was also observed in the subsequent tungsten divertor experiment). The higher W inventory in H-mode discharges may be caused by better particle confinement in this plasma phase. The decay time for the central tungsten concentration after laser ablation in ohmic discharges is about 80 ms. In H-mode plasmas with additional heating the decay time is usually about 120 ms. Some additionally heated discharges, however, showed very high particle confinement and the tungsten remained in the plasma for longer than 500 ms.

4.2 Quasicontinuum Intensity

For the investigation of the tungsten divertor experiment at ASDEX Upgrade the total tungsten radiation cannot be used, because the source of tungsten particles at the plasma boundary is continuous and the resulting radiation of W cannot be separated from the background radiation. Furthermore the detection limit of $c_W \geq 10^{-4}$ is not sensitive enough to be used for transport investigation under reactor relevant conditions. An alternative signal is the intensity of the quasicontinuum structure of tungsten measured by the grazing incidence spectrometer. An advantage of this structure is that it is emitted by tungsten ions of comparatively low ionization state, i.e. it can be observed in both ohmic and additional heated plasmas. However, it is a rather broad spectroscopic structure composed of the spectra of many ions, which renders the determination of its intensity more difficult. Simply monitoring the peak intensity at 5 nm may lead to incorrect results due to the additional radiation background in neutral beam heated discharges.

To get a quantitative measure for the quasicontinuum intensity it is essential to use the whole feature to achieve a sensitive detection limit. A linear regression is used to fit the grazing incidence spectrum in the wavelength region from 4 to 7 nm (averaged over 50 ms) by means of a set of sample spectra. Two of the spectra represent the quasicontinuum structure and the isolated lines of tungsten, respectively, three more spectra represent the lines of boron and carbon, which usually dominate the isolated lines in the observed wavelength region, and three additional spectra are used to model the changing background radiation of the plasma. The intensities of the spectra representing the W quasicontinuum structure and the isolated W lines will be denoted in the following $I_{W,qc}$ and $I_{W,il}$, respectively. The samples for the characteristic tungsten radiation were taken from the discharges #4955 and #4896, in which accumulation occured and in which the tungsten radiation could be well separated from the background radiation. A comparison between fitted and measured spectra for #8195 is shown in fig. 11. In this discharge the tungsten was not injected by means of laser ablation but is intrinsic, originating from the tungsten divertor plates in ASDEX Upgrade. The lower part of the figure shows the sample spectra, the upper part the observed and the fitted spectrum. A high particle confinement of the tungsten ions in the main plasma leads to a grazing incidence spectrum, in which both the isolated lines and the quasicontinuum structure can be seen.

To derive a tungsten concentration $c_{W,qc}$ from the spectroscopic measurements the quasicontinuum intensity, the quasicontinuum signal observed with the grazing incidence spectrometer was compared with the values of the tungsten concentrations derived by means of the bolometer measurements (previous subsection). In contrast to the bolometer method, the analysis of the grazing incidence spectrum cannot deliver $c_W(\rho)$-profiles but only a mean concentration $c_W(\rho_{L,qc}) = c_{W,qc}$ for the plasma layer in which the quasicontinuum-emitting ions exist (mean radius $\rho_{L,qc}$). Assuming that this layer has an effective thickness Δl, a constant emissivity of the quasicontinuum structure and a constant c_W the intensity of the quasicontinuum can be written as

$$I_{W,qc} = \int d\lambda \cdot \int dl \cdot \underbrace{n_e(l) \cdot c_W(l)}_{n_W(l)} \cdot n_e(l) \cdot \eta_{qc}(l,\lambda) \cdot cal_{GI}(\lambda) \tag{2}$$

$$= cal_{GI,qc} \cdot \bar{\eta}_{qc} \cdot n_e^2(\rho_{L,qc}) \cdot \Delta l(\rho_{L,qc}) \cdot c_{W,qc} \tag{3}$$

$$= \underbrace{cal_{GI,qc} \cdot \bar{\eta}_{qc} \cdot \Delta l_{norm}}_{cal_{qc,rel}} \cdot \mathcal{L}(\rho_{L,qc}) \cdot c_{W,qc} \cdot n_e^2(\rho_{L,qc}) \tag{4}$$

$I_{W,qc}$ is the intensity of the quasicontinuum observed by means of the grazing incidence spectrometer

in the wavelength region from from 4.5 nm to 7.0 nm in [counts/s]. $I_{W,qc}$ and therefore also $c_{W,qc}$ was only determined in discharge periods in which the grazing incidence spectrometer delivered unperturbed spectra. Especially the plasma phases in which the discharge was not at least for 100 ms in a divertor configuration were excluded because the multi channel plate detectors exhibit too large perturbations (probably caused by higher pressure in the spectrometer). The sensitivity of the instrument is given by $cal_{GI}(\lambda)$ and $\eta_{qc}(l,\lambda)$ summarizes the excitation and branching ratios of all transitions of the quasicontinuum in this wavelength region. The integration with respect to λ and l leads to an equation with mean values $cal_{GI,qc}$, $\bar{\eta}_{qc}$, $n_e^2(\rho_{L,qc})$, and $c_{W,qc}$ of the plasma layer located at ρ_L with a thickness of $\Delta l(\rho_{L,qc})$.

This thickness $\Delta l(\rho_{L,qc}) = \Delta l_{norm} \cdot \mathcal{L}(\rho_{L,qc}(T_{e,0}))$ varies with the central temperature because it is shifted outwards with increasing temperature in the core plasma. This dependence was approximated with the help of the simple model of the temperature dependence described in subsection 3.1 ((figure 2, the solid line shows $\mathcal{L}(T_{e,0})$).

The calibration factor $cal_{qc,rel}$ (which includes Δl_{norm}, $\bar{\eta}_{qc}$ and the sensitivity of the spectrometer) was obtained by comparing the maximum of

$$\frac{I_{W,qc}}{\mathcal{L}(T_{e,0}) \cdot n_e^2(\rho_{L,qc})} \tag{5}$$

after W laser ablation with the maximum central tungsten concentration $c_{W,bolo}$ obtained with the help of the bolometer method for several discharges (again parabolic n_e, T_e profiles were taken; for n_e the line averaged electron density $\bar{n}_e$ of the central DCN-interferometer-channel (H-1) was used; the difference between the actual density profile and $\bar{n}_e$ has only a small influence on c_W, because in ohmic discharges (with more peaked n_e profiles) the quasicontinuum is emitted in the central plasma and in H–mode discharges the electron profiles are usually flat.).

Figure 12 shows the relation between $c_{W,qc}$ and $c_{W,bolo}$ in which the calibration factor and $\mathcal{L}$ are already taken into account. The data points of almost all discharges are in a region defined by the two dashed lines indicating a 50% deviation from perfect agreement of the two concentration measurement methods (solid line). Larger deviations occur in H-mode-discharges in which the concentrations measurements can be disturbed by higher temperatures in the plasma center (strong decrease of p_W in for $T_{e,0}$ $\geq$1.5 keV) or hollow temperatures profiles (anomalous increase of Δl).

The relative error of $c_{W,qc}$ can be approximated by $\delta c_{W,qc} \approx \delta(n_e^2) + \delta\mathcal{L} + \delta I_{W,qc} + \delta cal_{qc,rel}$. The error of $\delta(n_e^2)$ is estimated to be 0.3 and the error of $\mathcal{L}$ can be estimates from fig. 2 to be about 0.5. The relative error $\delta I_{W,qc}$, calculated by means of the threefold standard deviation of $I_{W,qc}$ of the regression, was found to be about 20%. $\delta cal_{qc,rel}$ depends on the accuracy of the $c_{W,bolo}$-measurements. Because $cal_{qc,rel}$ was determined from several discharges (cf. fig. 12) due to averaging effects the influence of δn_e and δP_W (see determination of $c_{W,bolo}$) is much smaller and therefore $\delta cal_{qc,rel} \approx \delta p_W \approx 0.3$. These estimates result in a total error of $c_{W,qc}$ of $\delta c_{W,qc} \approx 1.3$. Additionally to these error estimates a detection limit was defined which results from the signal-to-noise-ratio of the grazing incidence spectrometer. From a comparison of several discharges with W laser ablation it was found to be $(5{\cdot}10^{-6}{\cdot}(4{\cdot}10^{19}m^{-3}/\bar{n}_e)^2)$, i.e. concentrations c_W below this detection limit are not expected to be reliable.

Figure 13 shows an example of the extracted $c_{W,qc}$ in a discharge with W laser ablation at 2.9 s. After 30 ms the W concentration at the center ($T_{e,0}$ $\approx$0.9 keV) reaches its maximum with $c_{W,qc}$ $\approx 10^{-4}$. The decay of the W signal follows an exponential decay with a time constant of about 100 ms. Even for $c_{W,qc}$ below the detection limit (dashed line) the exponential decay can be observed.

4.3 Isolated W lines

Due to the necessary modifications of the ADPAK ionization rates of W ions with charge numbers ≥ 30, which contribute to the calculations of p_W, there may be larger errors for p_W at higher temperatures. Furthermore, to detect smaller amounts of tungsten ($c_W \leq 10^{-4}$) in the center of hot plasmas, there is need for a spectroscopic method. The isolated lines of Br- to Cu-like tungsten, which are observed in the same λ region as the quasicontinuum, are suited to determine c_W in the central region of additional heated discharges. The intensity $I_{W^{45+}} = I_{W,\text{Cu-like}}$ of the line at 6.23 nm emitted by Cu-like tungsten is given (cf. equ. 3) by

$$I_{W^{45+}} = cal_{6nm} \cdot \eta_{W^{45+}} \cdot n_e^2(\rho_{L,W^{45+}}) \cdot \Delta l(\rho_{L,W^{45+}}) \cdot c_{W^{45+}}(\rho_{L,W^{45+}}) \quad (6)$$

with $\rho_{L,W^{45+}}$ the position of the maximum of the density of the copper like W ions, $\Delta l(\rho_{L,W^{45+}})$ the thickness of the corresponding plasma layer, $c_{W^{45+}}$ the concentration of the Cu-like W ions, and $\eta_{W^{45+}}$ is the theoretical emissivity for the line at 6.23 nm determined by means of the HULLAC code. With the help of the fractional abundance of these ions ($f_{W^{45+}} = c_{W^{45+}}/c_W$), calculated by means of the STRAHL-code, the total tungsten density is

$$c_W(\rho_{L,W^{45+}}) = \frac{I_{W^{45+}}}{cal_{6nm} \cdot \eta_{W45+} \cdot n_e^2(\rho_{L,W^{45+}}) \cdot \Delta l(\rho_{L,W^{45+}})} \cdot \frac{1}{f_{W^{45+}}} \quad (7)$$

To check the calibration factor cal_{6nm}, which was obtained by means of a double branching ratio methode (cf. sec. 2), an alternative calibration was performed which uses the intensity of the quasicontinuum structure. It is assumed that all radiation of the tungsten ions in the plasma region with $T_e \approx 0.8-1.$ keV is emitted in the quasicontinuum structure and that about 3/4 of this radiation is emitted into the 5 nm region (cf. [34]). With the help of the calculated radiation losses p_W another calibration factor cal_{bolo} of the grazing incidence spectrometer in the 4.5 nm–7.0 nm region can be deduced from a comparison of the observed intensity $I_{W,qc}$ and the deconvoluted bolometer measurements. Both calibration factors, cal_{6nm} and cal_{bolo}, agree within 20%. The value of 20% was therefore used to estimate the error of p_W and cal_{6nm}.

The total relative error for the determination of $c_W(\rho_{L,W^{45+}})$ is estimated to be $\delta c_W(\rho_{L,W^{45+}}) \approx \delta(n_e^2) + \delta\eta_{W^{45+}} + \delta I_{W^{45+}} + \delta cal_{6nm} + \delta\Delta l + \delta f_{W^{45+}} \approx 0.4 + 0.3 + 0.2 + 0.3 + 0.4 + 0.4 = 2.$ Further uncertainties may be introduced by accumulation of tungsten in MHD-structures. The estimate of $\delta\Delta l + \delta f_{W^{45+}}$ is expected to be too large, because the product $\Delta l \cdot f$ will vary less with varying ionization/recombination rates than Δl or f do.

To monitor the tungsten inventory in additionally heated plasmas the intensity $I_{W,il}$ of the sample of isolated W lines (cf. previous section), was calibrated by means of $c_W(\rho_{L,W^{45+}})$. This was done be comparison of $c_W(\rho_{L,W^{45+}})$ with $I_{W,il}$ during t=2.25 s–2.75 s in the discharge #8195 (cf. figure 14, hatched region). The resulting $c_{W,il}$ is an average value of the tungsten concentration c_W in the center of the plasma ($T_e \approx$2-2.5 keV). Due to the inclusion of a larger number of lines and a larger wavelength region this value is less sensitive to perturbations (e.g. blending of the Cu-like line with boron lines) than $c_W(\rho_{L,W^{45+}})$, which is determined by means of one single line.

4.4 Application to ASDEX Upgrade discharges

Figure 14 shows the time behaviour of $c_{W,il}$ and $c_{W,qc}$ (inset A) during an ASDEX Upgrade discharge with tungsten divertor (the grey shaded part indicates the detection limit during the discharge). Apart from the W concentration measurements time traces of the additional heating power (NBI, B), the electron

density and temperature (C, D), and the H_α-signal in the divertor (E) are shown. At 1.5 s the NBI is turned on and the discharges switches from L- to H-mode with better energy and particle confinement (see H_α-signal, ELM-signature). As a result of the improved confinement and the additional heating power in the main plasma $T_{e,0}$ and $\bar{n}_e$ increase. Due to higher particle and power fluxes to the tungsten divertor plates the erosion of W from the plates gets larger [35]. This increased tungsten influx in combination with the better confinement leads to an increase of c_W above the detection limit. 100 ms after start of neutral beam injection $c_{W,qc}$, which determines c_W at about ρ=0.7, reaches its maximum. Due to a lower transport in the main plasma, the tungsten ions need more than 200 ms to reach the plasma center (central $c_W = c_{W,il}$). Sawtooth-instabilities in the center lead to a modulation of the central W inventory (cf. $c_{W,il}$, inset A). After switch off of one NBI-source at 3.7 s the central temperature $T_{e,0}$ decreases below 1.5 keV and the higher ionized tungsten ions like Cu-like W recombine to ions with lower charge numbers. Therefore the $c_{W,il}$-signal, which determines c_W in regions with temperatures above 2 keV, falls below the detection limit. The W concentration in the layer with $T_e \approx 1$ keV, however, stays almost constant during the remaining NBI phase. The observed small decrease may be due to a reduced tungsten source in the divertor (smaller power flux to the divertor plates). After the last NBI source is switched off the H-mode changes to L-mode with lower particle confinement. Furthermore the W production in the divertor is reduced as a consequence of the decreased heating power. As a result the W inventory decreases and 200 ms after NBI shut down $c_{W,qc}$ falls below the detection limit.

5 Summary

The emission of tungsten in the wavelength region from 4 nm to 140 nm was investigated by W injection using laser ablation into ASDEX Upgrade plasma discharges. In ohmic discharges with electron temperatures up to $T_e \approx 1$ keV only the known W quasicontinuum at about 5 nm was observed. In discharges with additional heating and T_e up to 3 keV single W lines of Br- to Cu-like tungsten ions were observed. These lines occur in the two wavelength regions 4.5–7.0 nm and 12–14 nm. The identification of the lines was performed by means of HULLAC-code calculations. Especially a line at 13.35 nm was identified with a transition of the Zn-like W^{44+} ion.

The spatial distribution of the W ions was calculated with the help of ionization and recombination rates of the ADPAK-package and the transport code STRAHL. To obtain agreement between the observation of Br- to Cu-like lines in plasmas with $T_{e,0} \approx 2.3$ keV the ADPAK rates for ionization had to be increased by a factor of up to 3. This necessary increase can be explained by the effect of excitation autoionization.

Several methods were developed to determine the tungsten concentration c_W in discharges with temperatures from 1 to 3 keV at different locations in the plasma. In discharges with laser ablation the deconvoluted total radiation of tungsten was used to get a c_W-profile with a relative error of 0.8 for $c_W \geq 10^{-4}$. An improved method with lower detection limit was obtained by means of grazing incidence spectra in the 5 nm region. This method extends the concentration measurements to discharges with continuous source of tungsten like the tungsten coated divertor plates of the tungsten experiment at ASDEX Upgrade. The intensity of the W quasicontinuum was used to determine c_W in the plasma layer with $T_e \approx 1$ keV with a relative error of about 1.3 and a detection limit of about $5 \cdot 10^{-6}$ in ohmic discharges. In additionally heated discharges c_W was determined by means of the Br- to Cu-like W ions with a relative error of 2 in the plasma location with $T_e \approx$2-2.5 keV. A comparison of the methods used for the detemination of c_W shows that the obtained values of the tungsten concentration delivered by

these methods are consistent.

During the tungsten divertor experiment at ASDEX Upgrade c_W was monitored with the help of the spectroscopic methods presented [36]. The obtained spatial information of c_W will be used for further investigations of the transport properties of tungsten for different plasma configurations by means of the transport code STRAHL.

6 Acknowledgements

The authors like to thank D. Post for supplying the ADPAK rates for ionization and recombination. We are also grateful to the the ASDEX Upgrade team for expert running of the tokamak. The portion of this work performed at the Lawrence Livermore National Laboratory was carried out under the auspices of the U.S. Department of Energy under contract No. W-7405-ENG-48.

References

[1] G. Parker, R Janeschitz et al., J. Nucl. Mater. **241–243**, 1 (1997).

[2] C. García-Rosales, J. Nucl. Mater. **211**, 202 (1994).

[3] D. Post, R. Jensen, C. Tarter, W. Grasberger, and W. Lokke, Atomic Data and Nuclear Data Tables **20**, 397 (1977).

[4] V. Arunasalam et al., Recent results from the PLT tokamak, in *Proc. 8th Conf. EPS, Prague 1977*, volume 2, pages 17–28, 1978.

[5] R. Neu et al., Plasma Phys. Controlled Fusion **38**, A165 (1996).

[6] M. Klapisch, J. Schwob, B. Fraenkel, and J. Oreg, J. Opt. Soc. Am. **67**, 148 (1977).

[7] A. Bar-Shalom, M. Klapisch, and J. Oreg, Phys. Rev. A **38**, 1773 (1988).

[8] R. Neu et al., Behaviour of laser ablated impurities in ASDEX Upgrade discharges, 1995.

[9] E. Unger, Untersuchungen zur Absolutkalibration eines Grazing–Incidence–Spektrometers für Verunreinigungstransport an einem Fusionsexperiment, Technical Report IPP III/187, Max–Planck–Institut für Plasmaphysik, 1992.

[10] R. Fonck, A. Ramsey, and R. Yelle, Applied Optics **21**, 2115 (1982).

[11] R. Neu et al., accepted for publication in J. Phys. B .

[12] J. Fuchs, K. Mast, A. Herrmann, K. Lackner, and the ASDEX Upgrade Team, Proc. 21st EPS Conf. Control. Fusion ans Plasma Phys. ECA **18B**, 1308 (1994).

[13] T. A. Carlson, C. Nestor, N. Wassermann, and J. McDowell, Atomic Data **2**, 63 (1970).

[14] A. Bar-Shalom and M. Klapisch, Computer Phys. Comm. **50**, 375 (1988).

[15] M. Klapisch, Computer Phys. Comm. **2**, 239 (1971).

[16] I. P. Grant, J. Phys. B: At. Mol. Phys. **7**, 1458 (1974).

[17] K. B. Fournier, to appear in At. Data Nucl. Data Tables (September, 1997).

[18] M. Finkenthal, Phys. Lett. A **127**, 255 (1988).

[19] P. Mandelbaum, J. de Phys. Colloque C1 **49**, C1 (1988).

[20] J. Sugar, V. Kaufman, and W. Rowan, J. Opt. Soc. Am. B **10**, 1321 (1993).

[21] J. Sugar, V. Kaufman, and W. Rowan, J. Opt. Soc. Am. B **10**, 1977 (1993).

[22] J. Sugar, V. Kaufman, and W. Rowan, J. Opt. Soc. Am. B **10**, 799 (1993).

[23] R. Kelly, Journal of Physical and Chemical Reference Data **16**, 337 (1987).

[24] N. Acquista and J. Reader, J. Opt. Soc. Am. B **1**, 649 (1984).

[25] J. Reader and G. Luther, Phys. Rev. Lett. **45**, 1980 (1980).

[26] J. Seely, C. Brown, and W. Behring, J. Opt. Soc. Am. B **6**, 3 (1989).

[27] C. Brown et al., Atomic Data and Nuclear Data Tables **58**, 203 (1994).

[28] K. Behringer, Description of the impurity transport code STRAHL, Technical Report JET–R(87)08, JET Joint Undertaking, 1987.

[29] D. Mitnik, Phys. Rev. A **53**, 3178 (1996).

[30] D. Mitnik, Phys. Rev. A **55**, 307 (1997).

[31] R. Dux et al., Plasma Phys. Controlled Fusion **38**, 989 (1996).

[32] C. Breton, C. Michelis, M. Finkenthal, and M. Mattioli, Ionization Equilibrium of Selected Elements from Neon to Tungsten of Interest in Tokamak Plasma Research, Technical Report EUR–CEA–FC–948, Association EURATOM, CEA, 1978.

[33] G. Magyar et al., The laser blow-off system (KZ3) on JET, Technical Report JET-R(88)15, JET Joint Undertaking, 1988.

[34] E. Hinnov and M. Mattioli, Physics Letters **66A**, 109 (1978).

[35] A. Thoma et al., Spectroscopic measurements of the tungsten erosion in the ASDEX Upgrade divertor, to appear in PPCF, Nov. 1997.

[36] K. Asmussen et al., Investigations of tungsten in the central plasma of ASDEX Upgrade, in *Europhysics Conference Abstracts (Proc. of the 24th EPS Conference on Controlled Fusion and Plasma Physics, Berchtesgaden, 1997)*, edited by M. Schittenhelm, R. Bartiromo, and F. Wagner, volume 21A, part IV, Berchtesgaden, 1997, 24 th EPS.

[37] J. Reader and G. Luther, Physica Scripta **24**, 723 (1981).

[38] C. Breton, C. Michelis, and M. Mattioli, J. Quant. Spectrosc. Radiat. Transfer **19**, 367 (1978).

Appendix

A Tungsten lines in the EUV-region

Table 1: Observed transitions of tungsten ions around W^{28+}

Ion	transition	λ_{obs} [nm]	λ_{SKR} [nm]
W^{27} (Ag–like)	$4d^{10}4f\ ^2F_{5/2}$ – $4d^{10}4f(^1P)4f\ ^2D_{3/2}$ $4d^{10}4f\ ^2F_{7/2}$ – $4d^{10}4f(^1P)4f\ ^2D_{5/2}$	4.94	4.9403
W^{28} (Pd–like)	$4d^{10}\ ^1S_0$ – $4d^94f\ ^1P^\circ_0$	4.89	4.8948
W^{29} (Rh–like)	$4d^9\ ^2D_{5/2}$ – $4d^8(^3F)4f\ ^2F_{7/2}$	4.98	4.9785

- λ_{obs} denote the wavelengths observed at ASDEX Upgrade (uncertainty: 0.01 nm).
- The values for λ_{SKR} were taken from [20–22]

Table 2: Observed transitions of Br- to Cu-like W ions in the $\lambda \approx 5$ nm region

λ_{obs}	λ_{ref}	rel. meas. Intens	transition
4.69		45	W^{41+},W^{40+},W^{39+} (I.10,11,16,17,22,24)
4.72		42	W^{42+}(I.7)
4.79		40	W^{43+}(I.4)
6.06		47	W^{43+}, W^{41+}(I.5,12)
6.09	6.096 [24]; 6.0883 [26]	100	W^{44+}(I.2)
6.14		81	W^{43+}, W^{42+} (I.6,8)
6.23	6.2386 [37]; 6.2304 [26]	55	W^{45+}(I.1)
6.46		10	W^{39+}(I.26)
6.49		18	W^{41+}(I.13)
6.58		15	W^{40+}, W^{39+} (I.20,27)

- λ_{obs} denote the wavelengths observed at ASDEX Upgrade (uncertainty: 0.01 nm).
- The numbers in [] denote the corresponding reference.
- The numbers in () after the the ion symbols denote the corresponding transitions in table 3.

Table 3: Calculated transitions of Br- to Cu-like W ions in the $\lambda \approx 5$ nm region

no.	Ion	transition	λ_{calc} [nm]	calc. intensity†
I.1	W^{45+} (Cu–like)	$4s\ ^2S_{1/2}$ – $4p\ ^2P_{3/2}$	6.2128	8.6
I.2	W^{44+}	$4s^2\ ^1S_0$ – $4s4p\ ^1P_1$	6.0643	19.6
I.3	(Zn–like)	$4s4p\ ^1P_1$ – $4s4d\ ^3D_1$	7.3186	1.52
I.4	W^{43+}	$4s^24p\ ^2P_{1/2}$ – $4s^24d\ ^2D_{3/2}$	4.7594	9.89
I.5	(Ga–like)	$4s^24p\ ^2P_{1/2}$ – $4s4p^2\ ^2P_{1/2}$	6.0161	6.22
I.6		$4s^24p\ ^2P_{1/2}$ – $4s4p^2\ ^2P_{3/2}$	6.1159	6.14
I.7	W^{42+}	$4s^24p^2\ ^3P_0$ – $4s^24p4d\ ^3D_1$	4.6861	19.0

continued on next page

continued from previous page				
no.	Ion	transition	λ_{calc} [[nm]	calc. intensity[†]
I.8	(Ge–like)	$4s^24p^2\ ^3P_0$ – $4s4p^3\ ^3D_1$	6.1123	7.77
I.9	W^{41+}	$4s^24p^3\ ^4S_{3/2}$ – $4s^24p^24d\ J=1/2$	4.6587	2.89
I.10	(As–like)	$4s^24p^3\ ^4S_{3/2}$ – $4s^24p^24d\ J=3/2$	4.6621	7.76
I.11		$4s^24p^3\ ^4S_{3/2}$ – $4s^24p^24d\ J=5/2$	4.6976	7.99
I.12		$4s^24p^3\ ^4S_{3/2}$ – $4s4p^4\ ^4P_{3/2}$	6.0497	3.7
I.13		$4s^24p^3\ ^4S_{3/2}$ – $4s4p^4\ ^4P_{5/2}$	6.4853	4.67
I.14		$4s^24p^3\ ^4S_{3/2}$ – $4s^24p^24d\ J=5/2$	7.0440	1.05
I.15	W^{40+}	$4s^24p^4\ ^3P_2$ – $4s^24p^34d\ J=1$	4.6402	3.88
I.16	(Se–like)	$4s^24p^4\ ^3P_2$ – $4s^24p^34d\ J=2$	4.6518	6.92
I.17		$4s^24p^4\ ^3P_2$ – $4s^24p^34d\ J=2$	4.6543	8.92
I.18		$4s^24p^4\ ^3P_0$ – $4s^24p^34d\ J=1$	4.6598	3.19
I.19		$4s^24p^4\ ^3P_2$ – $4s4p^5\ ^3P_2$	6.2498	3.93
		(blended with: $4s^24p^4\ ^3P_0$ – $4s4p^5\ ^3P_1$)		
I.20		$4s^24p^4\ ^3P_2$ – $4s^24p^34d\ J=3$	6.5480	7.36
I.21	W^{39+}	$4s^24p^5\ ^3P_{3/2}$ – $4s^24p^44d\ J=5/2$	4.5886	1.41
I.22	(Br–like)	$4s^24p^5\ ^3P_{3/2}$ – $4s^24p^44d\ J=1/2$	4.6195	4.88
I.23		$4s^24p^5\ ^3P_{3/2}$ – $4s^24p^44d\ J=3/2$	4.6313	1.00
I.24		$4s^24p^5\ ^3P_{3/2}$ – $4s^24p^44d\ J=5/2$	4.6336	5.67
I.25		$4s^24p^5\ ^3P_{3/2}$ – $4s4p^6\ ^2S_{1/2}$	6.0688	2.65
I.26		$4s^24p^5\ ^3P_{3/2}$ – $4s^24p^44d\ J=5/2$	6.4145	9.40
I.27		$4s^24p^5\ ^3P_{3/2}$ – $4s^24p^44d\ J=3/2$	6.5293	4.72

[†]The intensities ([10^4 photons/ion/s]) were calculated with the assumptions:
T_e = 2000 eV, n_e = 10^{20} m^{-3}

B Used ionization and recombination rates

To get a simpler respresentaion of the data arrays of the ionization and recombination rates the data were fitted to equations similar to commonly used analytical formulae (cf. [38]). The fit was performed for an electron density of n_e=5 · 10^{19} m^{-3}. S is the ionization rate, α_r and α_{dr} are the rate coefficients for the radiative and dielectronic recombination, respectively. $\kappa_{a_s} = \frac{S}{S_{\mathrm{ADPAK}}}$ is the factor between the used ionization rates (showns in the following table) and the rates of the ADPAK packages [3]. q is the charge number of the corresponding W ion. Although the quantities of I_s, I_{rr}, E_{dr1} and E_{dr2} have [eV] as dimension they are simple fit parameters and must not identified with actual physical properties of the respective ion. The coefficients for all tungsten ions are shown in table 5

$$S = \frac{a_s}{T_e^{3/2}} \cdot \left[\frac{E_1\left(\frac{I_s}{T_e}\right)}{I_s/T_e} - \frac{b_s \cdot e^{c_s}}{I_s/T_e + c_s} \cdot E_1\left(\frac{I_s}{T_e} + c_s\right) \right] \cdot \quad 10^{-11}\ (\mathrm{eV})^{3/2}\ \mathrm{m^3 s^{-1}} \tag{8}$$

$$\alpha_r = \frac{a_{rr}}{\sqrt{T_e}} \cdot \frac{I_{rr}}{T_e} \cdot e^{I_s/T_e} \cdot E_1\left(\frac{I_{rr}}{T_e}\right) \cdot \quad 10^{-15}\ (\mathrm{eV})^{1/2}\ \mathrm{m^3 s^{-1}} \tag{9}$$

Table 4: Lines in the wavelength region from 12 nm to 14 nm which appear after tungsten laser ablation in the hot center of the plasma.

no.	λ_{obs}	λ_{calc}	λ_{pred} [27]	isolel. Sequ.	transition	type	rel. meas. intens.
II.1	12.19				2nd order of 6.06 nm (Table 2)		10
II.2	12.25				2nd order of 6.09 nm (Table 2)		19
II.3	12.33				2nd order of 6.14 nm (Table 2)		14
II.4	12.52				2nd order of 6.23 nm (Table 2)		8
II.5	12.70	12.627		Cu	$4s\ ^2S_{1/2}$ - $4p\ ^2S_{1/2}$	E1	52
II.6	12.78	12.706		Ga	$4s^24p\ ^2P_{1/2}$ - $4s4p^2\ ^4P_{1/2}$	E1	34
II.7	12.89	12.830		Se	$4s^24p^4\ ^3P_2$ - $4s^24p^4\ ^1D_2$	M1	33
II.8	13.00	13.057		Ge	$4s^24p^2\ ^3P_0$ - $4s^24p^2\ ^3P_2$	E2	31
II.9	13.18	13.237		As	$4s^24p^3\ ^4S_{3/2}$ - $4s^24p^3\ ^2D_{5/2}$	M1	20
II.10	13.35	13.399	13.2824	Zn	$4s^2\ ^1S_0$ - $4s4p\ ^3P_1$	E1	100
II.11	13.53	13.492		Se	$4s^24p^4\ ^3P_2$ - $4s^24p^4\ ^3P_1$	M1	40
II.12	13.59	13.710		Ge	$4s^24p^2\ ^3P_0$ - $4s^24p^2\ ^3P_1$	M1	35

- All wavelengths are given in [nm]. λ_{obs} are the wavelengths observed at ASDEX Upgrade, the wavelengths λ_{calc} were calculated by means of the HULLAC-code.
- The relative intensities were derived from the measured spectrum (cf. fig. 6).
- Agreement between the wavelength of lines with the corresponding 1st order wavelengths of table 2 can be obatained by shifting the wavelenghts of II.1–4 by 0.058 nm to shorter wavelengths and division by two. The same wavelength shift also leads to an agreement between the observed and the predicted wavelength at 13.2824 nm of II.10 [27].

$$\alpha_{dr} = \frac{1}{T_e^{3/2}} \cdot \left[a_{dr1} \cdot e^{-E_{dr1}/T_e} + a_{dr2} \cdot e^{-E_{dr2}/T_e} \right] \cdot \quad 10^{-11}\ (eV)^{3/2}\ m^3 s^{-1} \tag{10}$$

Table 5: Fit-coefficients for the used ionization and recombination rates

q	a_s	κ_{a_s}	b_s	c_s	I_s [eV]	a_{rr}	I_{rr} [eV]	a_{dr1}	E_{dr1} [eV]	a_{dr2}	E_{dr2} [eV]
0	0.848	1	0.0598	0.191	13.26	0	0	0	0	0	0
1	1.9	1	0.128	0.114	20.84	0.00188	9.259	0.00002	7.917	0.000118	117.4
2	2.2	1	0.053	0.0935	29.31	0.00309	12.72	0.000192	9.873	0.00321	134.8
3	2.26	1	0.0183	0.232	38.31	0.00472	15.8	0.000598	12.34	0.0144	116.9
4	2.34	1	0.113	0.096	47.31	0.00679	18.87	0.00104	13.2	0.0329	112.9
5	2.56	1	0.213	0.0153	57.1	0.00931	21.95	0.00153	13.84	0.0579	122.7
6	2.42	1	0.272	0.072	66.93	0.0123	25.3	0.00209	14.45	0.0886	136.9
7	2.42	1	0.389	0.0866	76.88	0.0157	28.98	0.00242	14.13	0.124	151.3
8	2.42	1	0.496	0.0895	87.1	0.0195	32.95	0.00277	14.34	0.165	166.5
9	2.4	1	0.578	0.0931	98.38	0.0238	37.28	0.00293	13.89	0.211	182.4
10	2.34	1	0.678	0.103	109.3	0.0284	41.95	0.00286	12.5	0.262	197.4
11	2.25	1	0.792	0.117	119.3	0.0336	46.95	0.00255	10.8	0.322	209.6
12	2.13	1	0.897	0.12	128.3	0.0391	52.34	0.0021	8.516	0.373	223.3
13	1.99	1	0.983	0.11	135.7	0.0451	58.07	0.00127	9.133	0.43	238.6

continued on next page

continued from previous page

q	a_s	κ_{a_s}	b_s	c_s	I_s [eV]	a_{rr}	I_{rr} [eV]	a_{dr1}	E_{dr1} [eV]	a_{dr2}	E_{dr2} [eV]
14	7.67	1	0.0702	0.132	433.9	0.0515	64.17	0.0492	208.2	0.46	279.3
15	7.5	1	0.0735	0.0926	470.2	0.0591	75.19	0.0907	217.8	0.499	311.6
16	7.36	1	0.0735	0.0733	508.9	0.0673	86.87	0.0951	212.3	0.578	338.4
17	7.23	1	0.159	0.121	541.9	0.0761	99.16	0.04	184.2	0.703	330.3
18	7.17	1	0.171	0.108	582.1	0.0855	112.1	0.0441	179.2	0.793	344.4
19	6.77	1	0.0372	0.11	630.4	0.0955	125.5	0.0604	176.4	0.864	368.7
20	6.61	1	0.0444	0.0886	671.3	0.106	139.6	0.075	172.5	0.946	389.2
21	6.35	1	0.0594	0.423	711.3	0.117	154.2	0.087	170.9	1.05	405.3
22	6.1	1	0.124	0.844	748.1	0.129	169.5	0.119	176.1	1.13	440.9
23	5.91	1	0.151	0.977	789.5	0.142	185.3	0.138	168.8	1.22	467.3
24	5.75	1	0.137	0.471	835	0.155	201.7	0.152	164	1.33	479.2
25	5.68	1	0.0963	0.167	884.7	0.168	218.6	0.187	161.2	1.41	525.6
26	5.28	1	0.0878	0.376	930.2	0.183	236.1	0.21	158.1	1.49	542.2
27	5.34	1	0.127	0.176	975	0.198	254.2	0.239	156.6	1.59	572.5
28	5.12	1	0.158	0.301	1018	0.213	272.8	0.269	155.1	1.69	604.2
29	5.08	1.02	0.17	0.16	1066	0.23	291.9	0.257	147.5	1.78	605.6
30	6.33	1.02	0.397	0.0749	1102	0.246	311.6	0.264	147.2	1.94	650.7
31	5.04	1.07	0.262	0.145	1154	0.264	331.9	0.279	145.6	2.01	705.6
32	5.66	1.28	0.198	0.106	1217	0.282	352.7	0.286	143.7	2.11	741.4
33	5.95	1.43	0.159	0.104	1274	0.301	374.3	0.292	140.6	2.21	779.1
34	5.75	1.49	0.119	0.114	1332	0.32	396.2	0.3	139.2	2.31	819.2
35	6.49	1.64	0.3	0.135	1368	0.34	418.7	0.309	140.6	2.41	860.4
36	6.6	1.84	0.351	0.241	1408	0.361	441.7	0.315	137.8	2.52	903.9
37	6.84	2.05	0.119	0.11	1522	0.383	465.3	0.323	137.6	2.57	921.2
38	7.36	2.22	0.433	0.189	1513	0.405	489.5	0.336	139	2.74	999
39	7.07	2.45	0.509	0.346	1550	0.427	514.2	0.308	129.9	2.83	1043
40	7.34	2.63	0.605	0.287	1585	0.451	539.5	0.288	129.7	2.93	1086
41	7.18	2.73	0.641	0.25	1644	0.475	565.2	0.262	128.5	3.06	1138
42	7.11	2.9	0.711	0.255	1697	0.5	591.6	0.23	122	3.13	1188
43	5.09	3.05	1.02	0.437	1535	0.525	618.5	0.198	117.2	3.23	1241
44	6.27	3.05	0.88	0.241	1790	0.551	645.9	0.165	112.4	3.32	1310
45	5.78	3.05	0.967	0.217	1847	0.578	673.9	0.0875	116.2	3.41	1351
46	14.9	3.11	0.0503	0.56	4131	0.606	702.4	2.62	1332	1.06	2426
47	13.7	3.05	0.193	0.731	4173	0.641	760.4	0.0197	229.4	3.43	1442
48	12.5	2.94	0.187	0.743	4294	0.676	819.2	0.0416	226.5	3.36	1472
49	11.6	2.9	0.18	0.767	4418	0.714	879.2	0.0622	227	3.28	1500
50	10.6	2.77	0.0615	0.374	4602	0.752	939.8	0.09	212.7	3.19	1532
51	9.37	2.63	0.103	0.638	4697	0.791	1001	0.104	207.3	3.09	1563
52	8.05	2.45	0.11	0.724	4818	0.832	1063	0.121	196.7	2.98	1593
53	7.09	2.3	0.0863	0.758	4963	0.874	1126	0.142	195.2	2.86	1632
54	5.76	2.09	0.0543	0.718	5103	0.917	1190	0.161	189.7	2.74	1680
55	5.39	2.01	0.125	0.182	5225	0.961	1254	0.18	182.8	2.61	1737
56	4.64	1.99	0.0776	0.313	5371	1.01	1320	0.197	176.4	2.51	1806
57	4.04	1.99	0.00969	0.388	5538	1.05	1386	0.155	114.6	2.31	1891
58	3.62	1.99	0.0822	0.373	5649	1.1	1454	0.147	106.8	2.16	1997
59	3.19	1.99	0.163	0.315	5763	1.15	1522	0.104	114.8	1.97	895.3
60	2.85	1.99	0.301	0.306	5850	1.2	1590	0.138	106.5	1.87	2305

continued on next page

continued from previous page

q	a_s	κ_{a_s}	b_s	c_s	I_s [eV]	a_{rr}	I_{rr} [eV]	a_{dr1}	E_{dr1} [eV]	a_{dr2}	E_{dr2} [eV]
61	1.78	1.99	1.02	1.31	5289	1.25	1660	0.126	94.88	1.7	2483
62	2.29	1.99	0.599	0.171	6078	1.3	1730	0.0993	86.89	1.58	2895
63	1.59	1.99	0.854	0.234	5919	1.36	1801	0.04	75.88	1.49	3457
64	4.2	1.99	0.372	13.8	15280	1.41	1873	1.43	4822	1.45	133100
65	3.77	1.99	0.0534	15.8	15650	1.5	2132	0.0114	173.2	1.34	4909
66	3.23	1.99	0.0691	11.6	15930	1.6	2392	0.00862	140.3	1.17	4924
67	2.66	1.99	0.21	5.22	16070	1.7	2653	0.0113	138	0.998	4952
68	1.72	1.99	1.14	2.68	14550	1.8	2911	0.0344	123.1	0.794	5001
69	1.6	1.99	0.209	4.7	16640	1.91	3169	0.00978	131.5	0.565	5063
70	0.757	1.99	1.21	1.39	13440	2.02	3428	0.0199	119	0.387	5131
71	0.446	1.99	1.09	1.74	14900	2.13	3684	0.00232	73.7	0.189	5234
72	1.27	1.99	0.0149	0.00149	73280	2.25	3938	0.0471	28020	6.88	503000
73	0.645	2	0.00972	0.000492	73890	2.79	7231	0.0253	29030	7.24	519800
74	0	0	0	0	0	3.38	9923	0	0	0	0

Figure 1:

Lines of sight of the used diagnostics for the investigation of the tungsten radiation in the central plasma of ASDEX Upgrade. Left side: SPRED and grazing incidence spectrometer; DCN-interferometer (channel H1→ $\bar{n}_e$) and Thomson Scattering system (T_e-profile). Right side: bolometer camera system (→ profile of the total radiation).

Figure 2:

Temperature dependence of the tungsten quasicontinuum signal as observed by the grazing incidence spectrometer (normalized to $\bar{n}_e$ and $c_{W,bolo} \cdot \bar{n}_e$ (measure for the amount of tungsten in the plasma). The solid line represents the temperature dependence of the thickness of the plasma layer, in which the W quasicontinuum is emitted.

Figure 3:

Tungsten quasicontinuum in a plasma with a central temperature of $T_{e,0}$=0.9 keV. Due to accumulation effects the central tungsten radiation after W laser ablation gets very strong, causing a hollow T_e-profile and a spreading of the region with Ag-, Pd, and Rh-like tungsten ions. This enables a clearer observation of lines of these ions (#4955, $\bar{n}_e \approx 7 \cdot 10^{19}$ m^{-3} , I_p=1 MA).

Figure 4:

Isolated tungsten lines after W laser ablation in an additionally heated plasma. The sawtooth shaped time dependence indicates, that the origin of the lines are highly ionized W-ions in the plasma center (#4896, additional heating: 7 MW NBI, $\bar{n}_e \approx 8 \cdot 10^{19}$ m^{-3}, $T_{e,0}$ ≈2.4 keV, I_p=1 MA).

Figure 5:

Spectrum of the observed tungsten single lines in the 6 nm region after tungsten laser ablation (#4896, 7 MW NBI, $\bar{n}_e \approx 8 \cdot 10^{19}$ m^{-3}, $T_{e,0} \approx 2.4$ keV, I_p=1 MA). Spectrum B was obtained from the spectra of the gracing incidence spectrometer (exposure time 5ms, averaged from 3.2 s to 3.3 s, the backround radiation (averaged from 2.6 s to 2.7 s) was subtracted). Spectrum A was used to calibrate the wavelength; spectrum C shows the identification of the lines by means of the HULLAC–code (element symbols indicate isoelectronic sequences).

Figure 6:

Lines of highly ionized tungsten in the 13 nm region after W injection at 2.5s (#7470, 5 MW NBI, $\bar{n}_e \approx 6 \cdot 10^{19}$ m^{-3}, $T_{e,0}$ ≈2.6 keV, I_p=1 MA).

A) Temporal behaviour of the lines as observed by the grazing incidence spectrometer → influence of central sawtooth activity. B) Time integrated spectra (Δt=100ms, 200ms after injection). C) Calculated Spectrum (RELAC-Code). Thick line: total intensity, thin lines: individual contributions of the Kr- to Ni-like W ions (with different offsets).

Figure 7:

Ionization rates for Cu- and Zn-like tungsten ions. Excitation-autoionization effects can explain the necessary increase by a factor of 2–3 of the ADPAK rates.

Figure 8:

Effect of a modification of ADPAK rates compared with original data for some W ionization states. The modification of the rates is necessary to explain the observation of lines of Cu-like tungsten in

additionally heated plasmas. A comparison with a pure coronal equilibrium (dashed dotted) shows the weak effect of transport (cf. sec. 3.3).

Figure 9:

Relative abundance of tungsten ions calculated by means of the transport code STRAHL and modified ADPAK rates for a typical additionally heated discharge (transport as in fig. 8, $T_{e,0}$ ≈2.6 keV). Br- to Ni-like W ions, which emit isolated lines, exist in the plasma center. W ions which are responsible for the W quasicontinuum structure at about 5 nm occur at the boundary of the main plasma (ρ_{pol} ≈0.8).

Figure 10:

Left side: radiation loss parameter calculated by means of ADPAK; right side: calculated tungsten inventory of the inner plasma ($\rho_{pol} \leq 0.6$) as a function of the injected amount of tungsten.

Figure 11:

Result of the determination of the intensity of the tungsten quasicontinuum by means of a regression using several sample spectra. Upper part: comparison of the original spectrum and result of the fit. Lower part: used sample spectra (W quasicontinuum, isolated W lines, lines of B and C, shapes of the background).

Figure 12:

Averaged tungsten concentration calculated from the intensity of the W quasicontinuum as a function of the central tungsten density determined from of the bolometer measurements; the dotted lines show the 50% deviation limits from the ideal agreement.

Figure 13:

Temporal behaviour of the tungsten concentration after tungsten laser ablation at 2.9s in an ohmic discharges (#4542 , $\bar{n}_e \approx 4 \cdot 10^{19}$ m^{-3}, $T_{e,0}$ ≈0.9 keV, I_p=0.8 MA). After about 30 ms the concentration in the center reaches it maximum and decays afterwards with a decay time of about 100 ms. The dashed line marks the detection limit.

Figure 14:

Example of an ASDEX Upgrade discharges with moderate tungsten inventory (#8195). Increased confinement of the main plasma (H-mode) and W erosion at the W divertor plates lead to a W concentration above the detection limit (grey shaded in inset A) after start of NBI. The switch off of one NBI source leads to a decrease of $T_{e,0}$ and the highly ionized W ions recombine (decrease of $c_{W,il}$). After the switch off of the last NBI source the confinement and the W erosion at the W plates decrease (L-mode and lower T_e at the divertor plates, respectively) and the tungsten diffuses out of the plasma. The hatched region was used to calibrated the intensity of the fit results for the sample of isolated W ions to obtain $c_{W,il}$.

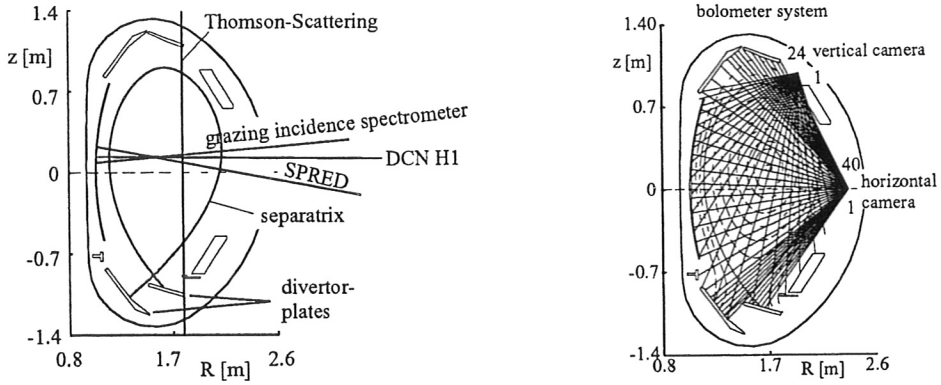

Figure 1:

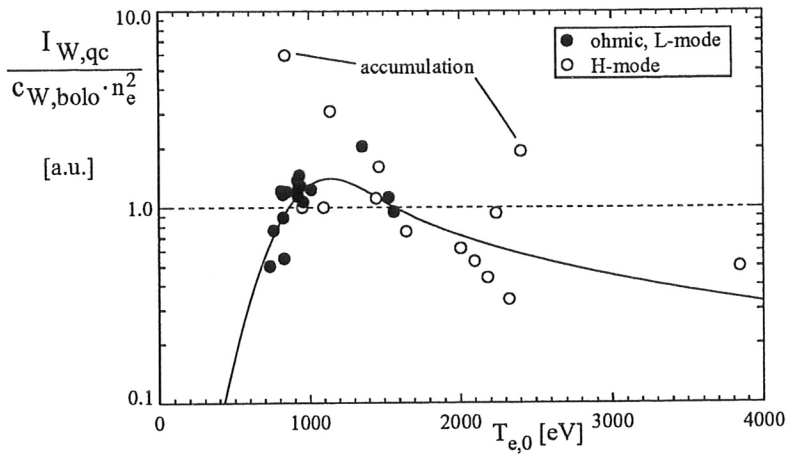

Figure 2:

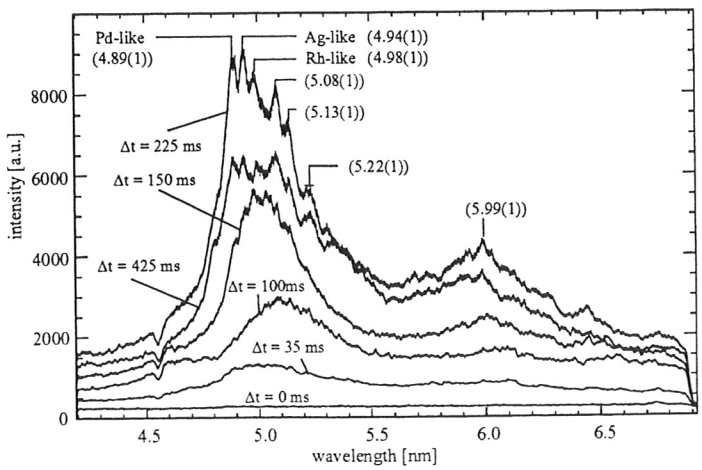

Figure 3:

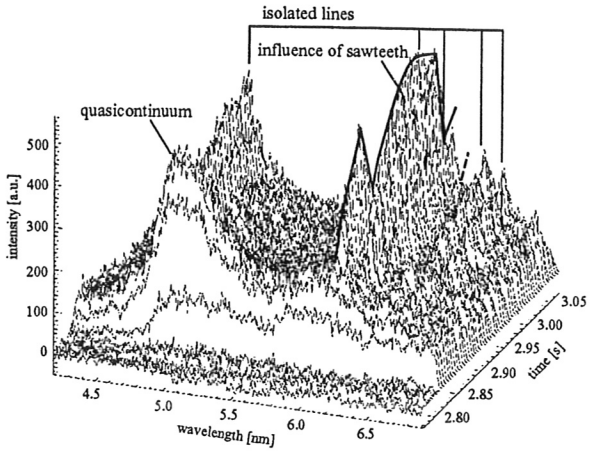

Figure 4:

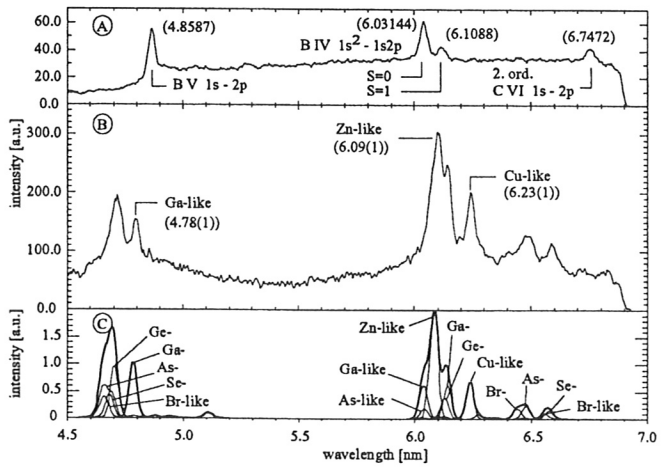

Figure 5:

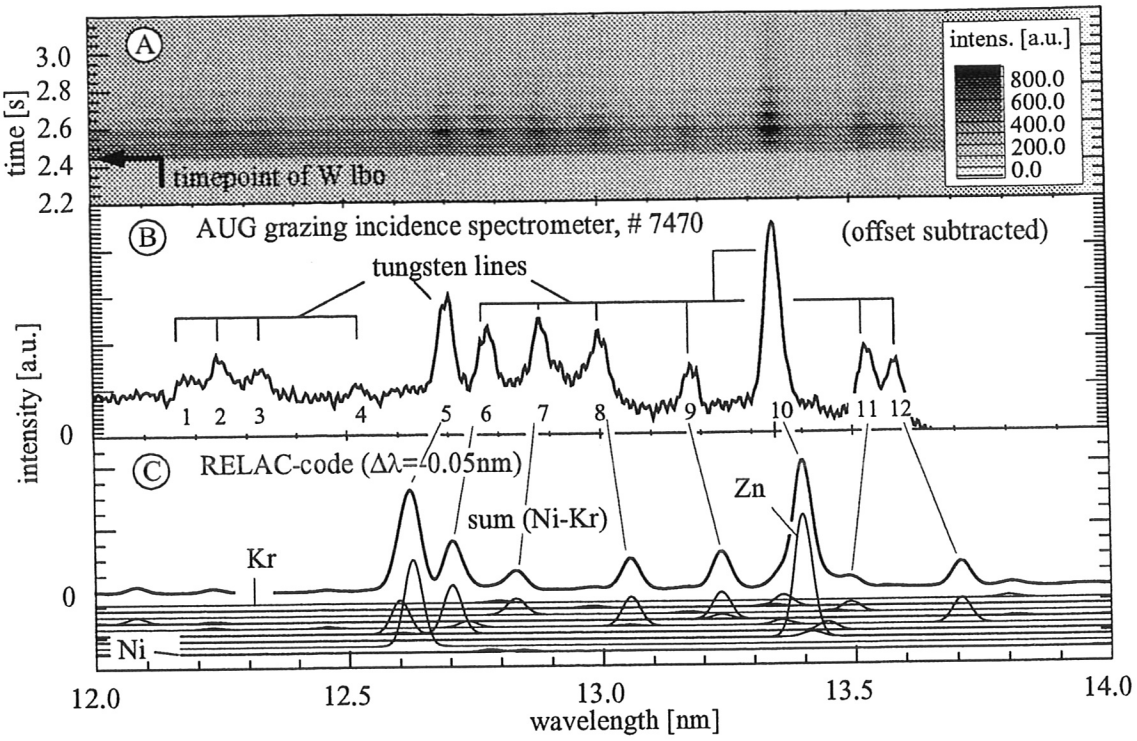

Figure 6:

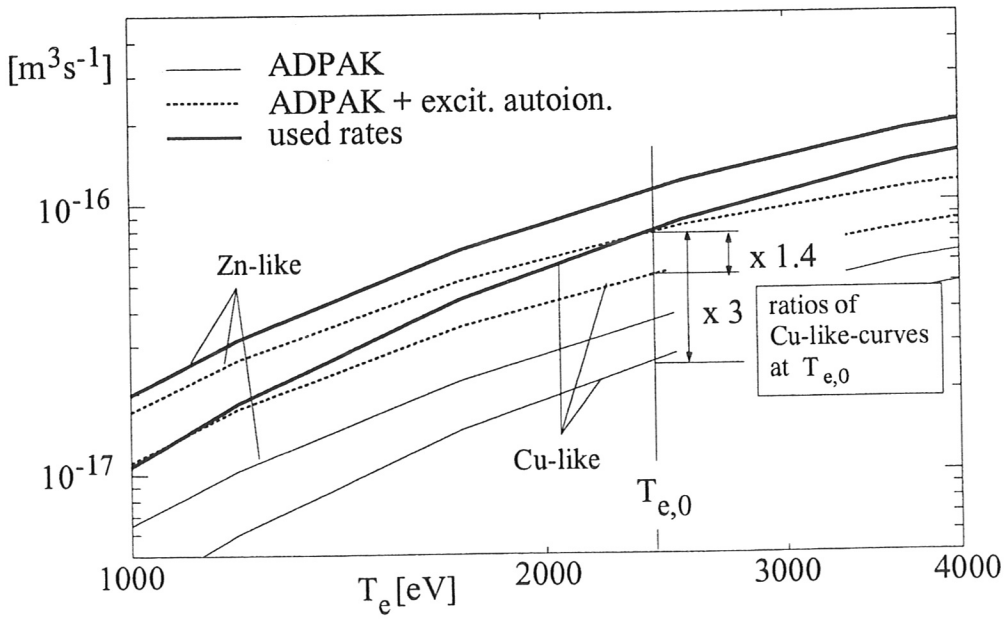

Figure 7:

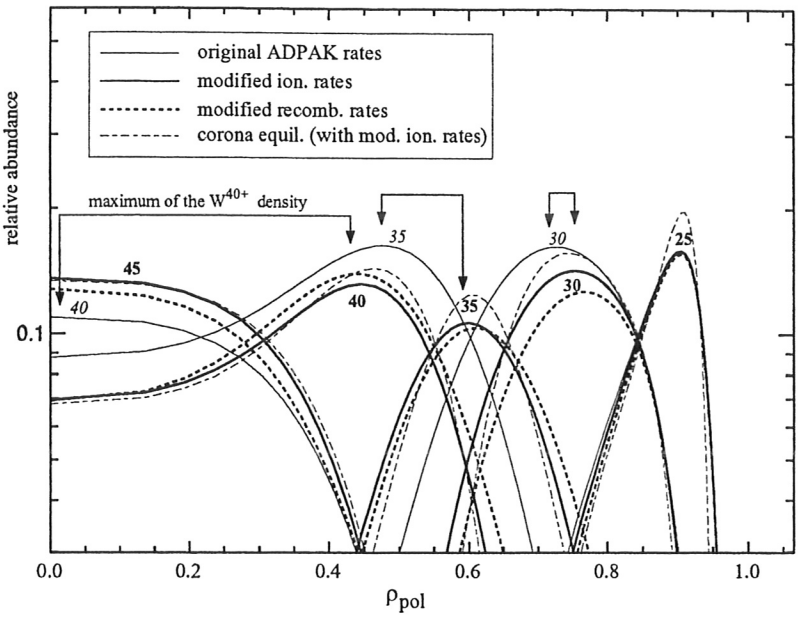

Figure 8:

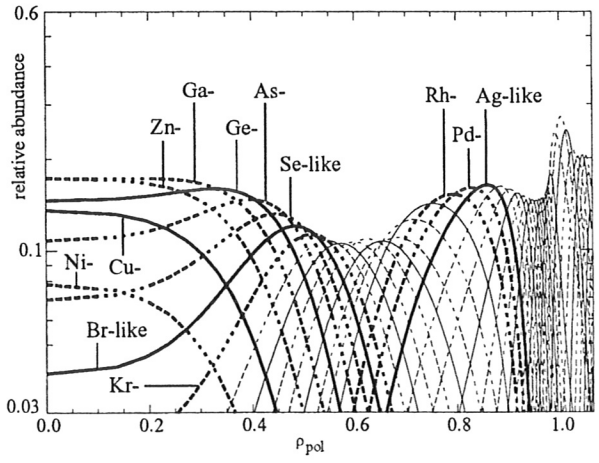

Figure 9:

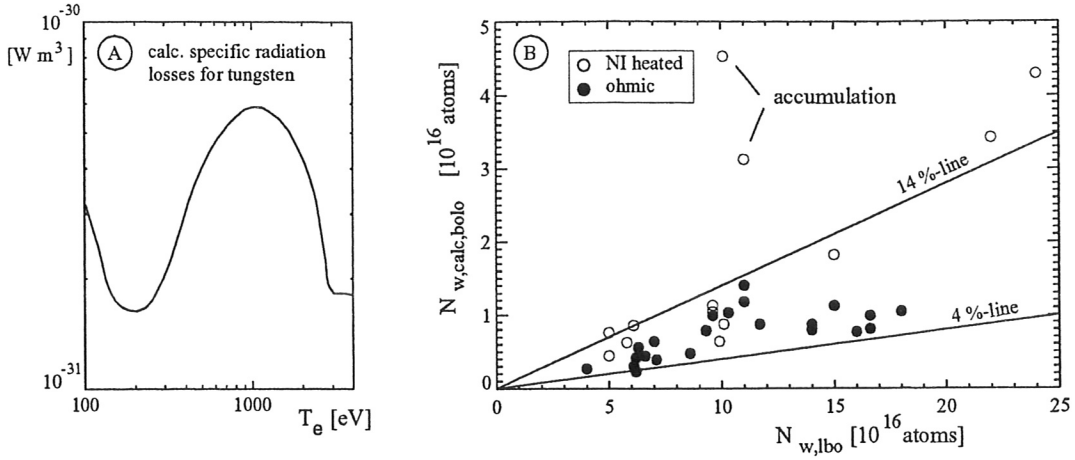

Figure 10:

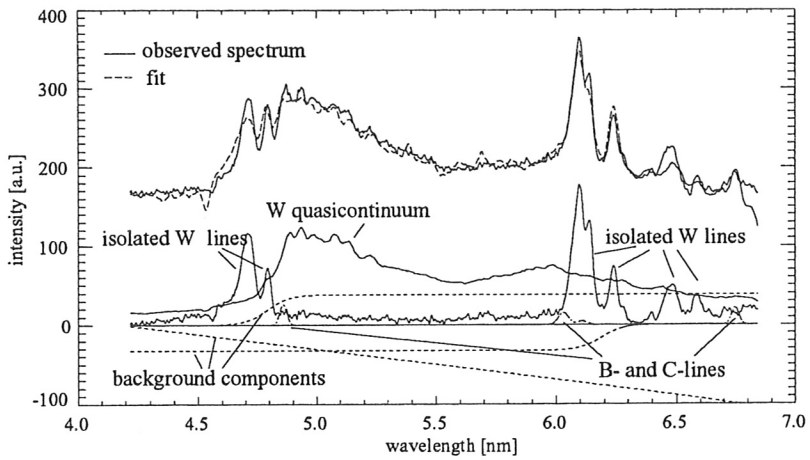

Figure 11:

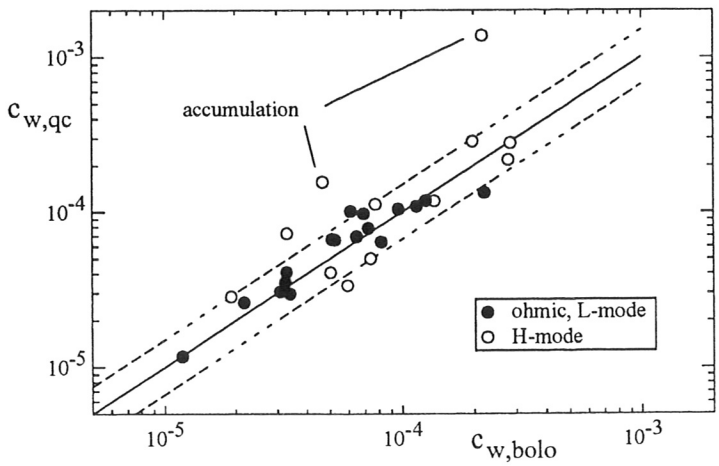

Figure 12:

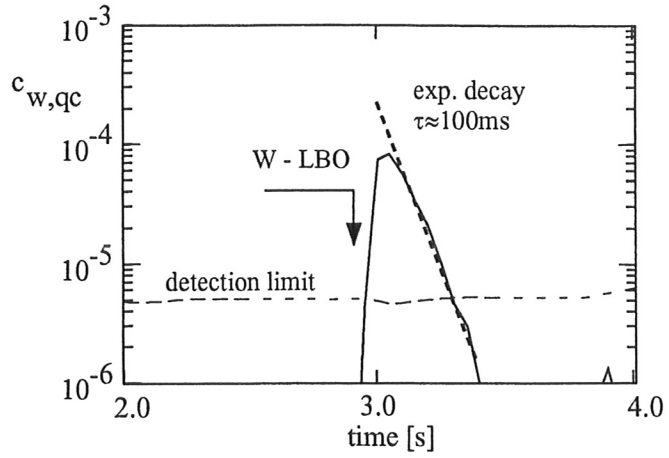

Figure 13:

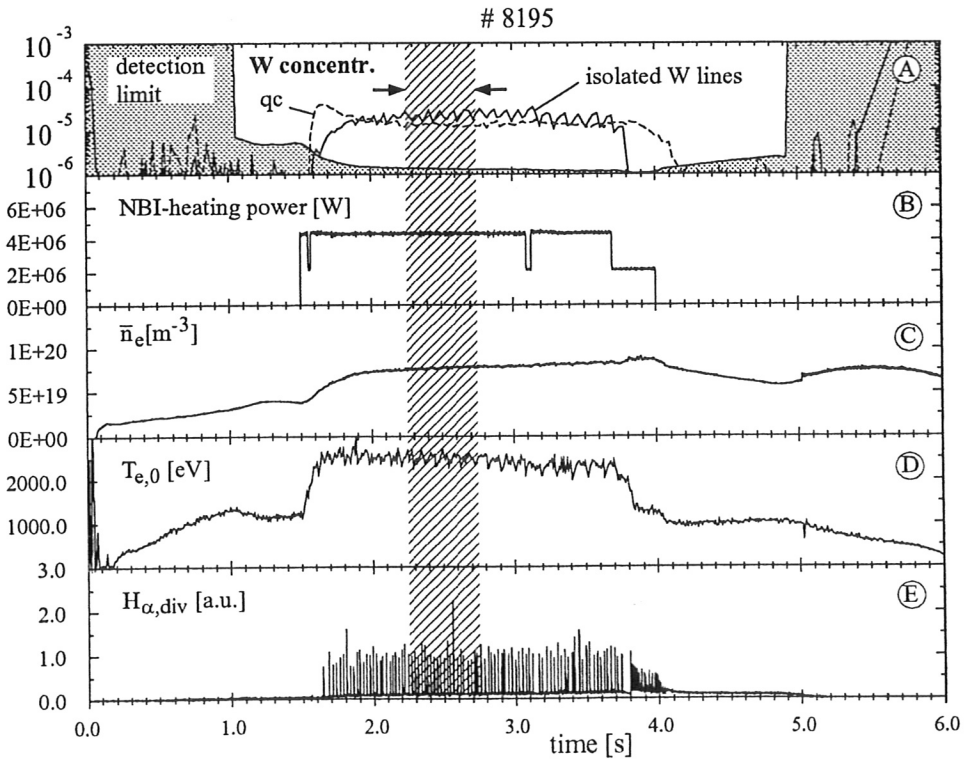

Figure 14: